Am J Nucl Med Mol Imaging 2024;14(4):272-281
www.ajnmmi.us /ISSN:2160-8407/ajnmmi0158097

Original Article

Accurate brain pharmacokinetic parametric imaging using the blood input function extracted from the cavernous sinus

Yafen Kang[1*], Zixiang Chen[2*], Zhuoyue Song[3], Yaping Wu[4,5], Zhenxing Huang[2], Yuxi Jin[2], Ting Zhang[6], Meiyun Wang[4,5], Zhanli Hu[2], Yang Yu[1]

[1]*School of Pharmaceutical Sciences, Guangzhou University of Chinese Medicine, Guangzhou 510006, Guangdong, China;* [2]*Lauterbur Research Center for Biomedical Imaging, Shenzhen Institute of Advanced Technology, Chinese Academy of Science, Shenzhen 518055, Guangdong, China;* [3]*Bioengineering Laboratory, Institute of Biological and Medical Engineering, Guangdong Academy of Sciences, Guangzhou 510006, Guangdong, China;* [4]*Department of Medical Imaging, Henan Provincial People's Hospital and People's Hospital of Zhengzhou University, Zhengzhou 450003, Henan, China;* [5]*Institute for Integrated Medical Science and Engineering, Henan Academy of Sciences, Zhengzhou 450000, Henan, China;* [6]*Shenzhen Talent Institute, Shenzhen 518071, Guangdong, China.* [*]*Equal contributors.*

Received May 28, 2024; Accepted August 8, 2024; Epub August 25, 2024; Published August 30, 2024

Abstract: Brain pharmacokinetic parametric imaging based on dynamic positron emission tomography (PET) scan is valuable in the diagnosis of brain tumor and neurodegenerative diseases. For short-axis PET system, standard blood input function (BIF) of the descending aorta is not acquirable during the dynamic brain scan. BIF extracted from the intracerebral vascular is inaccurate, making the brain parametric imaging task challenging. This study introduces a novel technique tailored for brain pharmacokinetic parameter imaging in short-axis PET in which the head BIF (hBIF) is acquired from the cavernous sinus. The proposed method optimizes the hBIF within the Patlak model via data fitting, curve correction and Patlak graphical model rewriting. The proposed method was built and evaluated using dynamic PET datasets of 67 patients acquired by uEXPLORER PET/CT, among which 64 datasets were used for data fitting and model construction, and 3 were used for method testing; using cross-validation, a total of 15 patient datasets were finally used to test the model. The performance of the new method was evaluated via visual inspection, root-mean-square error (RMSE) measurements and VOI-based accuracy analysis using linear regression and Person's correlation coefficients (PCC). Compared to directly using the cavernous sinus BIF directly for parameter imaging, the new method achieves higher accuracy in parametric analysis, including the generation of Patlak plots closer to the standard plots, better visual effects and lower RMSE values in the K_i (P = 0.0012) and V (P = 0.0042) images. VOI-based analysis shows regression lines with slopes closer to 1 (P = 0.0019 for K_i) and smaller intercepts (P = 0.0085 for V). The proposed method is capable of achieving accurate brain pharmacokinetic parametric imaging using cavernous sinus BIF with short-axis PET scan. This may facilitate the application of this imaging technology in the clinical diagnosis of brain diseases.

Keywords: Dynamic PET, brain pharmacokinetic parametric imaging, blood input function, cavernous sinus, Patlak graphical model

Introduction

Dynamic positron emission tomography (PET) of the brain, accompanied by pharmacokinetic parametric analysis derived from the acquired dynamic PET images, is pivotal for the early and precise diagnosis of brain cancers and neurological diseases [1-6]. To this end, one of the most widely used analytical methods is based on the Patlak graphical model [7-9], in which analyzers acquire the blood input function (BIF) from the vessels of the descending aorta in the reconstructed dynamic PET images [10-12]. Patlak quantitative parametric imaging of the net metabolic flux, K_i, and the distribution volume of free molecules, V, are achieved based on the dynamic PET images as well as the extracted BIFs [13, 14].

However, for most PET imaging systems with short axial fields of view (FOVs), dynamic images of the beds of the lung and brain cannot be acquired in a single scan; under such conditions, pharmacokinetic parametric imaging of the brain must use the BIF extracted from the patient's head region. However, as illustrated in **Figure 1**, Patlak graphical parametric imaging using a head BIF (hBIF) suffers from limited accuracy, because 1) the time-activity curves (TAC) of the head vessel BIFs (carotid artery or cavernous sinus) have nonnegligible differences from those of the descending aorta BIFs (aBIF) (**Figure 1B**) and 2) head vessels are smaller, and the limited number of effective voxels on the PET images leads to an extracted hBIF with an unsatisfactory signal-to-noise ratio. The limited accuracy of brain parametric imaging (**Figure 1D**) seriously hinders its clinical application in the diagnosis and analysis of brain diseases. For PET imaging systems with short axial FOVs, therefore, it is of great importance to explore methods for accurate Patlak graphical model-based parametric imaging method using hBIFs.

Long-axis PET imaging systems such as the Siemens Biograph Vision Quadra, PennPET Explorer and UIH uEXPLORER are able to provide lung and head dynamic PET images in one scan [15-17], which facilitate investigations of Patlak parametric imaging methods using hBIFs. One

https://doi.org/10.62347/LSYG1380

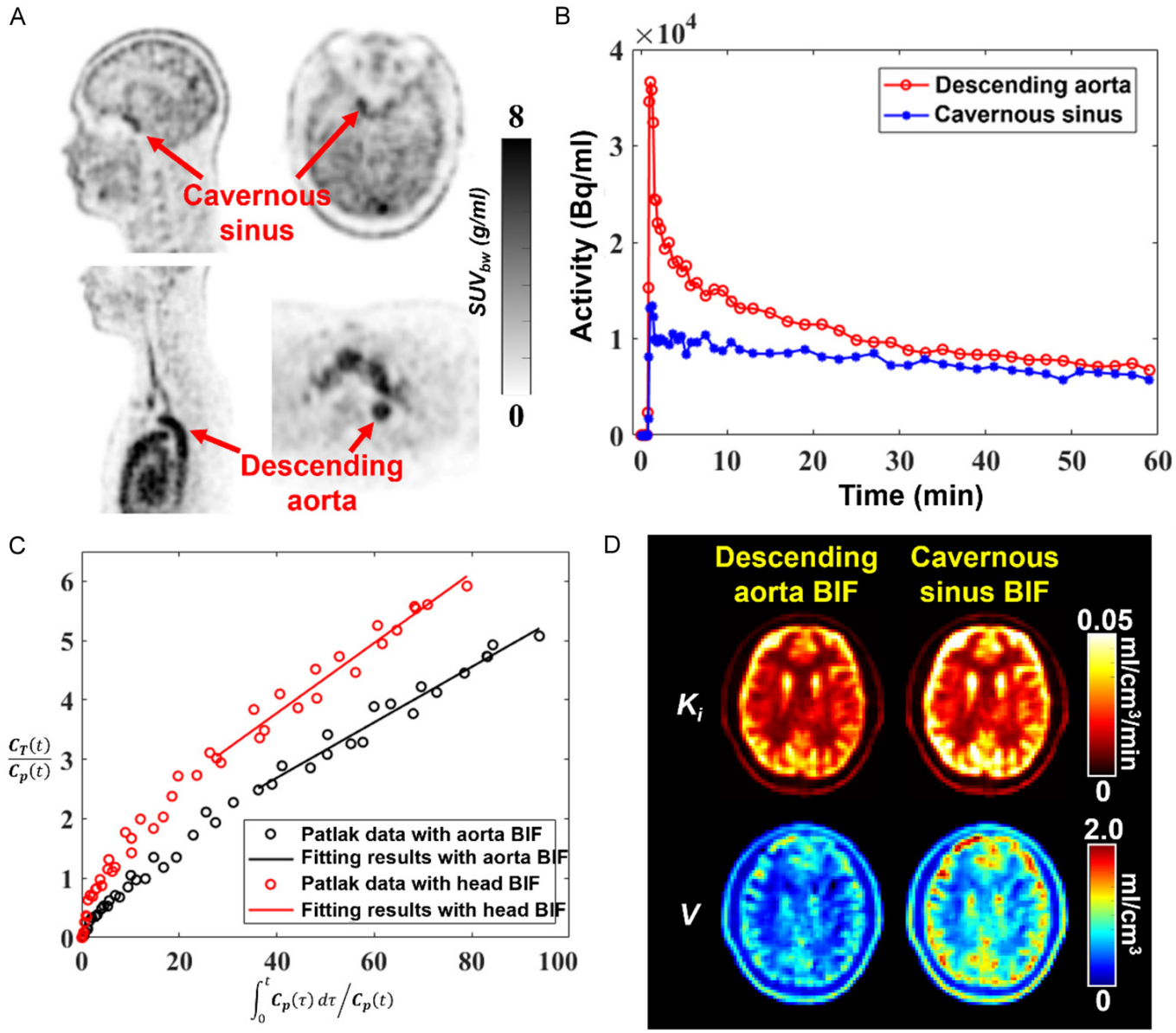

Figure 1. Pharmacokinetic parametric imaging using a cavernous sinus BIF. A. The location and morphology of the cavernous sinus and descending aorta; B. Differences between the aBIF and cavernous sinus hBIF; C. Differences between Patlak plots acquired based on the hBIF and aBIF; D. Differences between Patlak parametric images acquired based on the hBIF and aBIF.

potential strategy involves creating a model that transforms the hBIF to a standard aBIF by analyzing and comparing the morphological and statistical features, such as peak values, time to peak, averages, and exponential decay patterns, of the two BIFs when measured in a single dynamic PET scan. Another avenue is the application of machine learning models to directly derive an aBIF from a given hBIF. The above two ideas have a certain degree of feasibility; however, the validity of their statistical analysis or learning is highly dependent on the establishment of a large dynamic PET dataset. The feasibility will be diminished if the clinical whole-body dynamic PET database is not suitably large. Finding a method that is less dependent on dataset size to achieve accurate Patlak graphical model-based parametric imaging based on hBIF would be of greater clinical importance.

The cavernous sinus consists of both arteries and veins, as well as some nervous tissues [18, 19], and its positional and morphological characteristics are easily recognizable (as shown in **Figure 1A**). The current study explores a method to achieve accurate Patlak parametric imaging based on hBIFs extracted from the cavernous sinus. The proposed method is established based on the mechanism of the Patlak graphical model. The key points include 1) finding the integral value of the early-stage BIF curve via linear fitting; 2) correcting the late-stage curve of the hBIF based on the mean difference in BIFs; and 3) building a modified equation for the Patlak graphical model. The rest of this paper is organized as follows: Section 2 presents the details of the proposed method, Section 3 describes the parametric imaging experiments conducted in this study, and Section 4 shows the results of our

parametric imaging experiments and related discussions. Finally, we give the conclusions of this study in Section 5.

Material and methods

Pharmacokinetic parametric imaging based on the Patlak graphical model

The classical Patlak graphic model is specifically used for pharmacokinetic parametric imaging of irreversible tracers such as ^{18}F-fluorodeoxyglucose (^{18}F-FDG), which is currently the most common PET imaging agent for diagnosing cancer diseases in clinical practice [20-22]. The goal of Patlak parametric imaging is to acquire the K_i and V images that represent the net glucose metabolic flux and the distribution volume of the free glucose molecules, respectively. Based on the acquired dynamic PET imaging data, K_i and V are calculated by fitting the following equation:

$$\frac{C_T(t)}{C_p(t)} = \frac{\int_0^t C_p(\tau)\,d\tau}{C_p(t)} \cdot Ki + V \ \#(1)$$

Where $C_T(t)$ and $C_p(t)$ are the tissue time-activity concentration curve (TAC) and BIF, respectively. Eq. (1) is also named the Patlak plot, in which the section corresponding to the last 30-40 minutes of the dynamic PET scan is approximately linear and is used for linearly fitting K_i (that is, the slope of the linear plot) and V (the intercept of the linear plot), as shown in **Figure 1C**. By voxelwise calculation, one can acquire the parametric images that are registered to the original PET images.

To derive our proposed method, the Patlak model shown by Eq. (1) is modified to

$$\frac{C_T(t)}{C_p(t)} = \frac{E + \int_{t^*}^t C_p(\tau)\,d\tau}{C_p(t)} \cdot Ki + V \ \#(2)$$

Where E is the integral value of the early-stage BIF, namely,

$$E = \int_0^{t^*} C_p(\tau)\,d\tau \ \#(3)$$

This section ($0 \le t \le t^*$) corresponds to the early stage of the PET scan, where t^* is approximately 20-30 minutes; over this period, the Patlak plot is nonlinear. t^* is the start time of the late stage of the PET scan, which yields a linear Patlak plot section.

Fitting the integral value of the early-stage BIF

The first step of the proposed method is to find the early-stage integral value of the standard (descending aorta) BIF, E_a, based on the measured head (cavernous sinus) BIF integral value, E_h. We may reasonably assume a linear relationship between E_a and E_h:

$$E_a = k \cdot E_h + b \ \#(4)$$

Then, by collecting a certain number of data pairs, k and b can be acquired by simple linear fitting. The predicted integral value corresponding to a new E_h is acquired as follows:

$$E_{pred} = k \cdot E_h + b \ \#(5)$$

Late-stage BIF correction

According to Eq. (2), after acquiring the early-stage integral value of the predicted BIF, we need only the late-stage BIF corresponding to the linear section of the Patlak plot to calculate K_i and V. As shown in **Figure 3B**, there exists a marked difference between the late-stage sections of the hBIF, $C_{p,h}$, and those of the aBIF, $C_{p,a}$; therefore, we need a prediction process to achieve

$$C_{p,h}(t)|_{t \ge t^*} \Rightarrow C_{p,a}(t)|_{t \ge t^*} \ \#(6)$$

$C_{p,h}$ and $C_{p,a}$ have similar tendencies in the phase of $t \ge t^*$; therefore, we may assume a simple relationship between them in this phase:

$$C_{p,a}(t)|_{t \ge t^*} = C_{p,h}(t)|_{t \ge t^*} + A \ \#(7)$$

Constant A can be acquired by finding the mean difference (MD) between the late-stage $C_{p,h}$ and $C_{p,a}$, namely,

$$MD = \sum_{n=1}^{N} \frac{\int_{t^*}^{t^{end}} \left(C_{p,a}^n(t) - C_{p,h}^n(t)\right) dt}{\int_{t^*}^{t^{end}} 1 dt} \Big/ N \ \#(8)$$

Where t^{end} is the end time of the scan and N is the number of dynamic PET datasets used to find the MD. Based on Eq. (8), we have

$$C_{p,pred}(t)|_{t \ge t^*} = C_{p,h}(t)|_{t \ge t^*} + MD \ \#(9)$$

Patlak parametric imaging using the new model

Based on Eq. (2), (5) and (9), the Patlak graphical model can be rewritten as

$$\frac{C_T(t)}{C_{p,pred}(t)} = \frac{E_{pred} + \int_{t^*}^t C_{p,pred}(\tau)\,d\tau}{C_{p,pred}(t)} \cdot Ki + V \ \#(10)$$

According to Eq. (10), the Patlak plot used for fitting K_i and V is only displayed for data points corresponding to $t \ge t^*$. The global flowchart of the proposed parametric imaging method is shown in **Figure 2**. In summary, the calculation of K_i and V based on the head BIF, $C_{p,h}(t)$, is carried out via the following steps: a) Estimating the early-stage aorta BIF integral value, E_{pred}, via Eq. (5), with the coefficients, k and b, acquired from the previous data fitting; b) Correcting the late-stage BIF and acquiring the estimated $C_{p,pred}(t \ge t^*)$ via Eq. (9), with MD obtained from the average of the late-

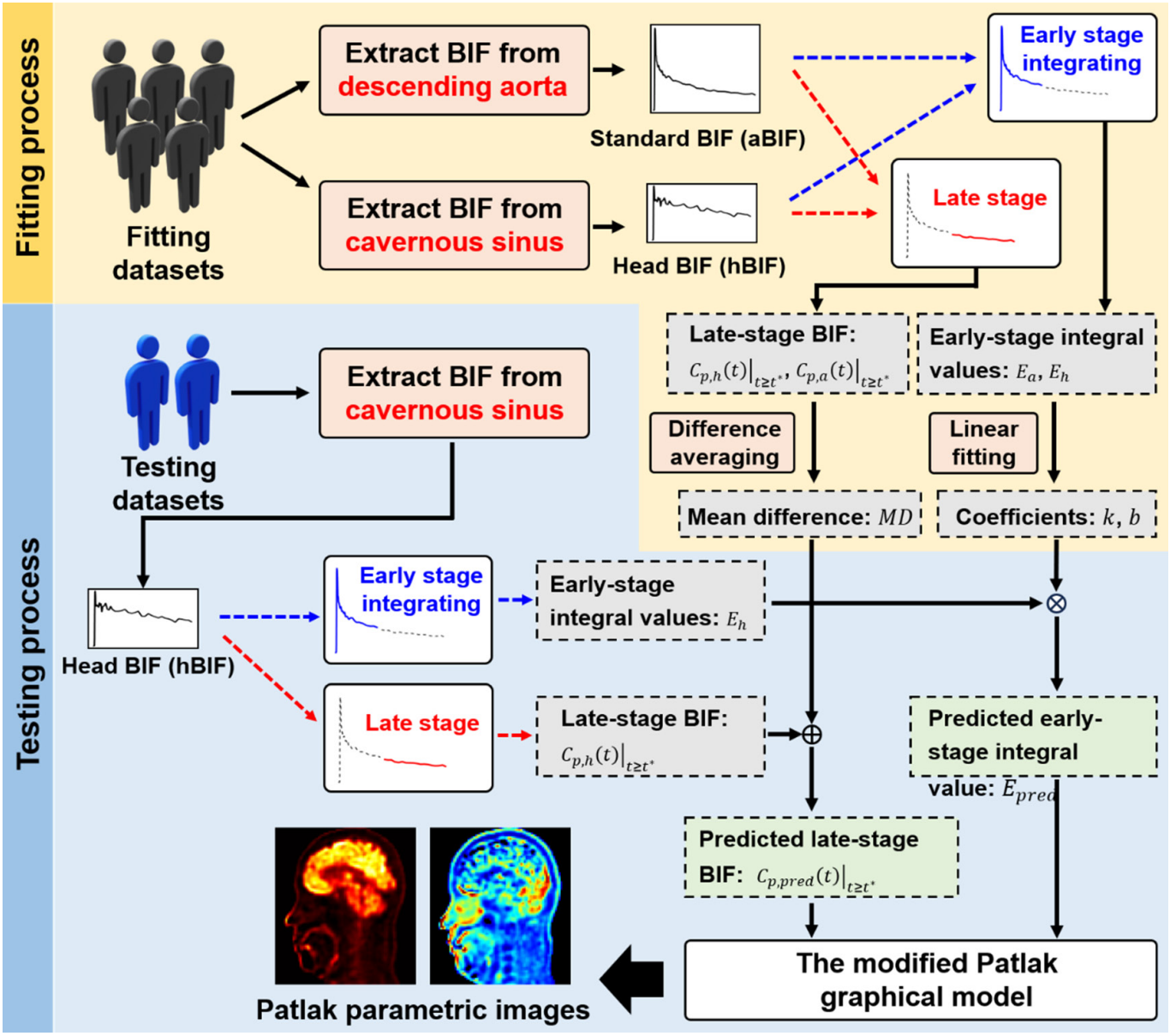

Figure 2. Flowchart of the current study.

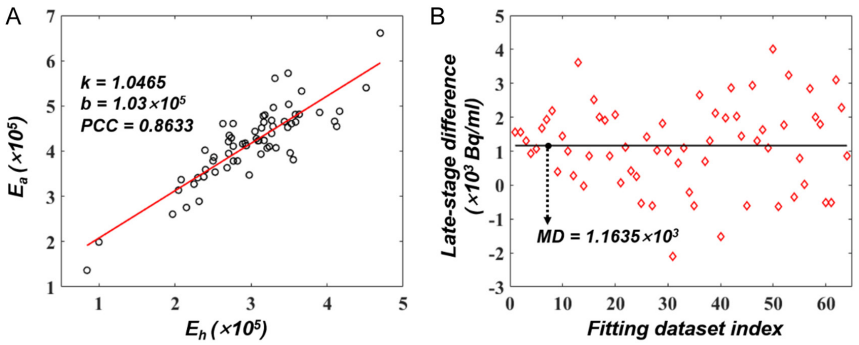

Figure 3. Results of early-stage BIF integral value fitting and late-stage BIF mean difference calculation. A. Fitting result between E_h and E_a; B. Averaging the deviations between the late-stage hBIF and aBIF to calculate the *MD*.

stage BIF deviations; c) Voxelwise calculation of the Patlak graphical model data based on Eq. (10) and acquisition of K_i and V images via linear fitting.

Experiments

Clinical ^{18}F-FDG dynamic PET data

Following approval by the committee of medical ethics of Henan Provincial People's Hospital, the dynamic PET imaging data of 67 patients were used for brain pharmacokinetic parametric imaging experiments in this study. Dynamic PET images were acquired using the uEXPLORER PET/CT imaging system (United Imaging Healthcare Inc.). The dynamic scan lasted for approximately one hour after the injection of ^{18}F-FDG, and the resulting imaging data were divided and reconstructed into 56 frames (5 s × 12, 10 s × 6, 30 s × 8, 60 s × 6 and 120 s × 24). PET images were reconstructed via the 3D time-of-flight (TOF) ordered-

subset expectation maximization (OS-EM) method [23] with 3 iterations and 20 subsets. The included datasets contain neither remarkable motion-induced brain image artifacts nor framewise misalignments. Imaging experiments were conducted using only 90 slices of images that covered the head region of the patients.

BIFs are acquired from the dynamic reconstructed PET images. A reference image frame temporally located at approximately 250 s post injection is used to sketch the regions of the descending aorta and cavernous sinus. This guarantees that the normally high uptake of brain region will not affect the proposed method since at the time point of 250 s post injection, FDG have not arrived the high metabolic level region.

Experiment implementations

The flowchart of the current study is given in **Figure 2**. The whole database established in this study contains 67 dynamic PET series, in which the data of 64 patients (95% of the database) are used for fitting k and b (in Eq. (5)) and finding MD (in Eq. (8)). The remaining 3 datasets (5% of the database) are used for testing the established model shown by Eq. (10). The fitting-testing process was repeated 5 times; each time, the data were divided into the fitting and testing sets randomly, and, therefore, the model was tested with a total of 15 patient datasets.

Based on visual observation of the generated Patlak plots, the time region corresponding to the linear section is defined as $24<t\leq60$ minutes after tracer injection, that is, $t^* = 24$ minutes. In other words, the early stage of the dynamic scan is defined as the first 24 minutes of the scan, while the late stage refers to the later 36 minutes of the scan. According to the time protocol used in this study, this linear section corresponds to the last 18 frames of the dynamic PET images. The Patlak graphical pharmacokinetic parameters are calculated in a voxelwise manner to acquire the K_i and V images, which are then registered to the reconstructed PET images.

Evaluation methods

In this study, we evaluated the proposed parametric method both qualitatively and quantitatively. The evaluation methods include:

1) Voxel-level Patlak plot comparison. This method will show whether the cavernous sinus BIFs can yield Patlak plots that are similar to the standard plots and reveal how the proposed method helps improve the accuracy of Patlak graphical model fitting to acquire K_i and V.

2) Parametric image visual inspection. The pharmacokinetic parametric images yielded by the proposed method and those directly calculated based on the original Patlak graphical model using an hBIF are qualitatively compared.

3) Root-mean-squared-error (RMSE) measurement. RMSEs are calculated for all the tested datasets to evaluate whether the proposed method can stably provide higher K_i and V imaging accuracies based on an hBIF. For every tested dataset, 30 slices that include the main intracerebral region are measured slice by slice and averaged to acquire the global RMSE. Paired t-test, one of the most widely understood, approved and used statistical analysis method to figure out the significance of difference between two groups of data or signal, is conducted to figure out the significance of that the new method brings RMSE reduction, p-value less than 0.05 indicates the significance [24, 25]. In this process, parametric images acquired with the standard aBIFs are applied as the reference.

4) VOI-based accuracy measurement. 5 × 5 × 5 VOIs are extracted from the calculated K_i and V images using both the original model and the proposed method. 15 arbitrarily selected intracerebral voxels, corresponding to the 15 tested datasets, respectively, are assigned to be the VOI centers. The relative absolute error (RAE) of the VOIs with respect to the standard images are plotted in a voxelwise manner, and the linear regressions, as well as the Person's correlation coefficients (PCCs) [26] between the K_i and V values in the VOIs yielded by the hBIFs and aBIFs, are displayed. Paired t-test is applied to the regression coefficients. The RAE is defined by

$$RAE = \frac{\left|\Phi_{refer} - \Phi\right|}{\Phi_{refer}} \#(11)$$

Where Φ_{refer} and Φ are the reference and calculated parameter values, respectively. The PCC is calculated by

$$PCC = \frac{1}{N-1}\sum_{i=1}^{N}\left(\frac{VOI_i - \overline{VOI}}{\sigma}\right)\left(\frac{VOI^{refer}_i - \overline{VOI^{refer}}}{\sigma_{refer}}\right) \#(12)$$

Where VOI and VOI^{refer} are the VOIs extracted from the calculated and reference K_i or V images, respectively. $\overline{VOI}$ denotes the mean of the VOI. σ and σ_{refer} are the standard deviations of VOI and VOI^{refer}, respectively.

Results

In this section, we describe our experimental results using the proposed Patlak parametric imaging method with the cavernous sinus BIF. For convenience, the tested datasets are labeled from #1 to #15. To provide a comprehensive evaluation, we showcase results from various datasets in this section. The result of the linear fitting between E_h and E_a, as well as the acquisition of MD, for one of our implementations are shown in **Figure 3**. According to **Figure 3A**, the acquisition of E_{pred} relies more on the fitted intercept, b, while the slope, k, is close to 1. The acquired MD is positive, which means that the late-stage aBIF is likely to be of higher intensity than the aBIF. Taking both the facts that $MD>0$ and $b>0$, $k>1$ into consideration, we

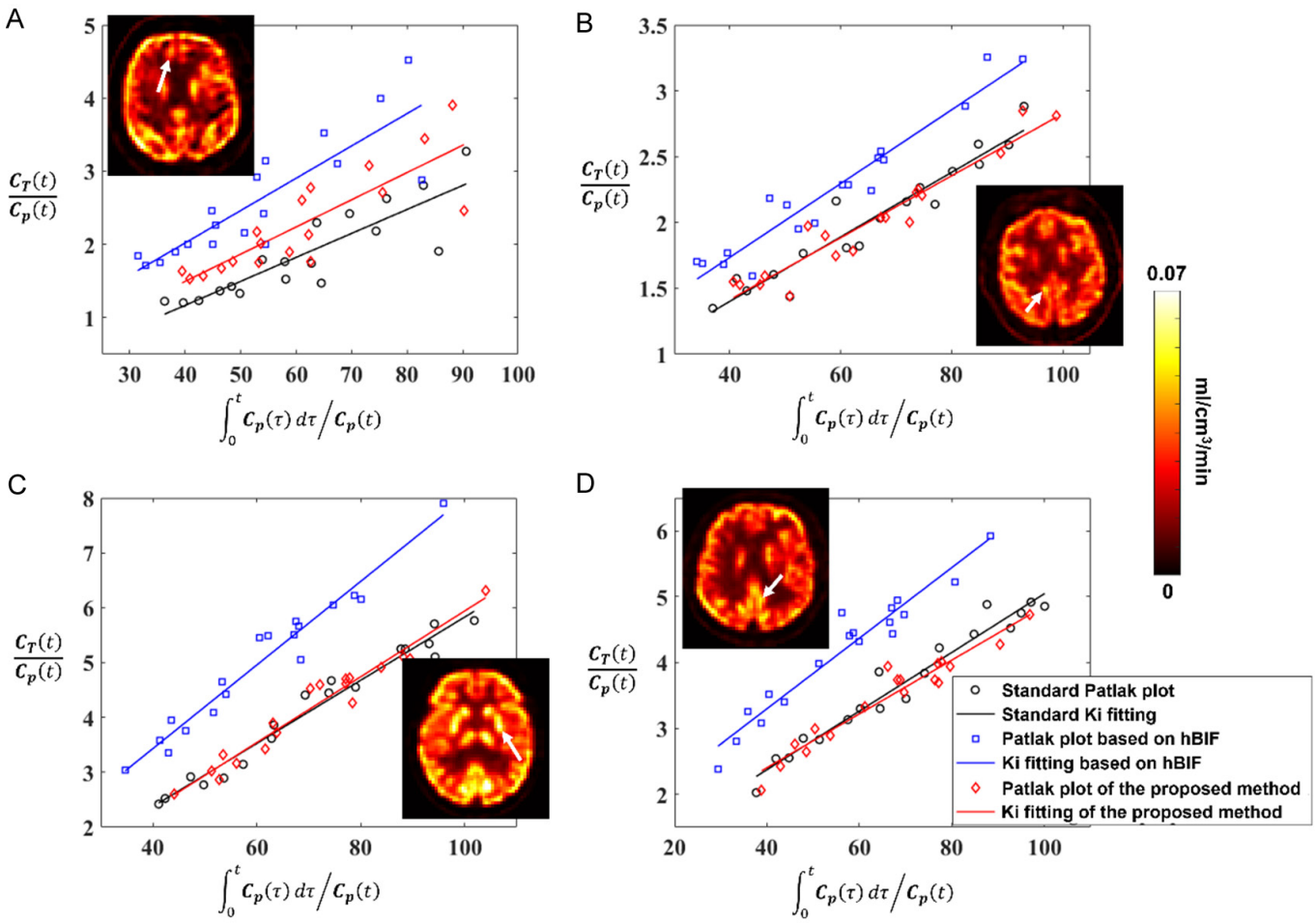

Figure 4. Voxel-level Patlak plots within the linear section for four of the tested datasets. (A-D) correspond to tested datasets #5, #7, #10 and #14, respectively. The corresponding voxel locations are indicated by the white arrows in the subfigures.

see that the hBIF extracted for the cavernous sinus is likely an underestimated BIF for pharmacokinetic parametric analysis using the Patlak graphic model, which results in overestimations in the intensities of the computed K_i and V images.

Voxel-level Patlak plots

Voxel-level Patlak plots of four of the tested datasets (Datasets #5, 7, 10 and 14) are shown in **Figure 4**. Voxels are extracted from the intracerebral region, as depicted by the subfigures. Notably, using the cavernous sinus hBIFs, the proposed method is able to provide Patlak plots that align more closely to the standard cases than the original Patlak model. This is the mechanism of the proposed method for obtaining more precise K_i and V values for every single voxel and for further generating parametric images with higher accuracies.

Visual inspection of K_i and V images

The calculated K_i images of testing patient datasets #2, 6 and 15 are shown in **Figure 5**, while the V images are shown for datasets #3, 8 and 12 in **Figure 6**. Using the hBIFs, the Patlak parametric images generated by the proposed method are qualitatively similar to the corresponding standard images obtained with aBIFs. As previously discussed, the calculated K_i and V images are prone to have overestimated intensities when using a cavernous sinus hBIF. Our method mitigates such overestimations by adjusting the hBIFs within the Patlak graphical model, thereby achieving precise parametric imaging in the absence of a standard aBIF.

RMSE measurements

The global RMSEs of the calculated K_i and V images of all the tested patient datasets are given in **Figure 7**. These values are calculated from 30 image slices that cover the main intracerebral regions from among the 3D parametric images. According to **Figure 7**, for most of the tested datasets, the proposed method is able to provide lower global RMSE values, indicating the effectiveness of accurate Patlak graphical parametric imaging using a cavernous sinus hBIF of the proposed method (P = 0.0012 and 0.0042 for K_i and V, respectively). However, due to the limited size of the fitting database, there are instances in which the new model cannot produce better K_i or V images in the testing process.

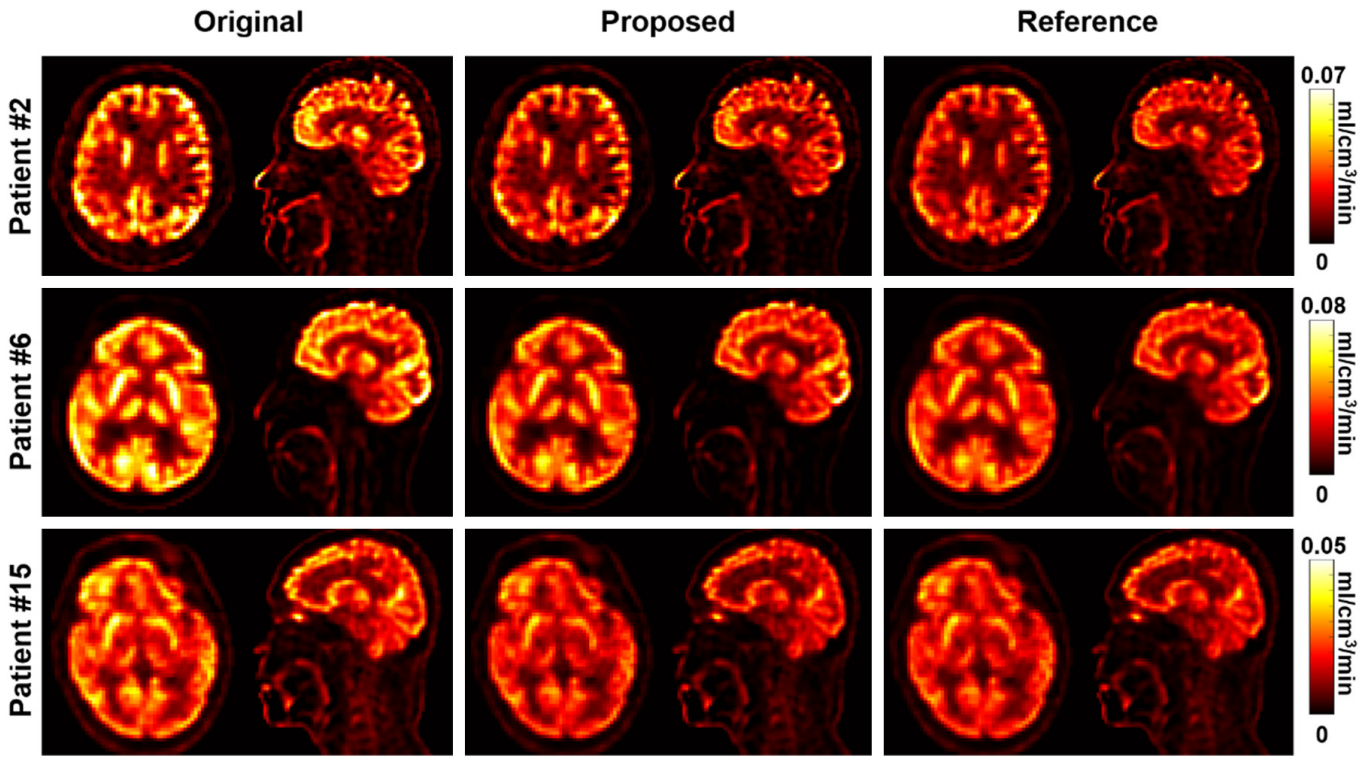

Figure 5. Brain K_i images of tested datasets #2, #6 and #15 acquired by the original Patlak model and the proposed method using cavernous sinus hBIFs. The reference images are the K_i images obtained with standard aBIFs.

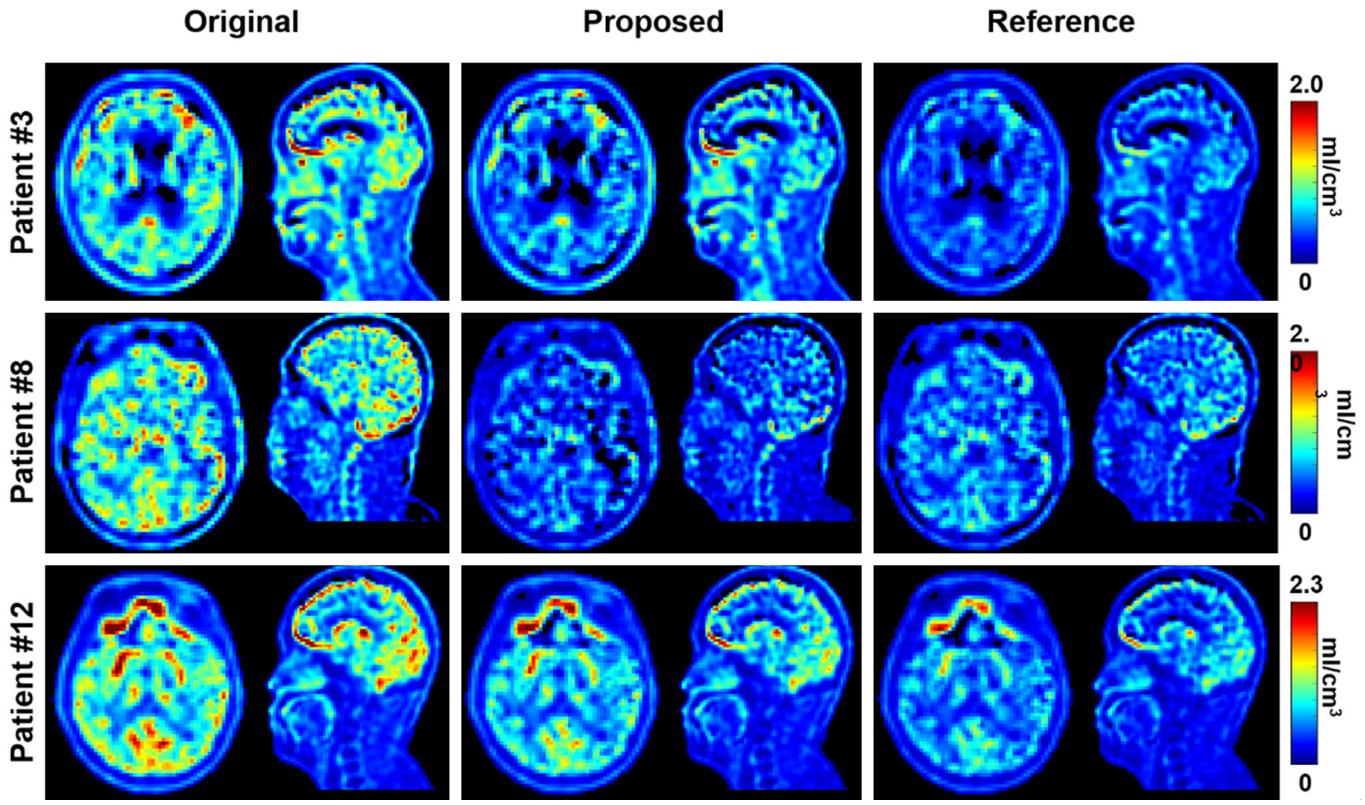

Figure 6. Brain *V* images of tested datasets #3, #8 and #12 acquired by the original Patlak model and the proposed method using cavernous sinus hBIFs. The reference images are the *V* images obtained with standard aBIFs.

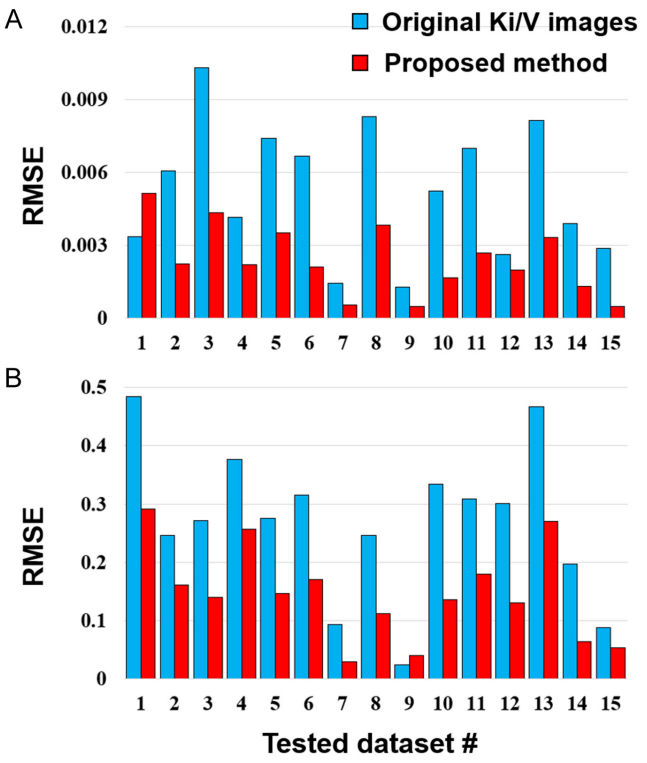

Figure 7. Global RMSE values calculated between the hBIF and aBIF-based parametric images. (A and B) are for K_i and V images, respectively. The displayed values are acquired upon averaging 30 slices that include the main intracerebral region.

VOI-based accuracy measurement

The VOI-based analysis is carried out to quantitatively evaluate the accuracy of the Patlak parametric images in more detail. The results for tested patient datasets #5 and 14 are shown in **Figure 8**. The RAEs between the hBIF- and aBIF-based Patlak parameter values are calculated voxelwise in the 5 × 5 × 5 VOI. The central locations of the analyzed VOIs are indicated by the subfigures. The RAEs of the K_i and V values calculated by the new method are remarkably smaller than those obtained by the original Patlak model, and the proposed method effectively decreases the error in the K_i and V calculations by using a cavernous sinus hBIF (**Figure 8A**, **8B**, **8E** and **8F**).

The fitting results between the calculated and standard values also demonstrate the performance of the proposed method. For the two showcased datasets, as illustrated in **Figure 8C**, **8D**, **8G** and **8H**, the fitting slopes (k) derived from our method tend to be closer to 1 than those from the original model, and the intercepts (b) are notably reduced. This quantitatively demonstrates the higher accuracy in estimating K_i and V by using the proposed method. For the whole testing set, by using the proposed method, k values of the K_i VOIs are closer to 1 ($P = 0.0019$) and b values of the V VOIs are smaller ($P = 0.0085$). PCC values for all the cases are sufficiently large, indicating that the pharmacokinetic parameters calculated based on cavernous sinus BIFs are highly correlated to the standard values. K_i and V imaging using a cavernous sinus BIF is therefore reliable if the accuracy is guaranteed.

Discussions

Size of the fitting database

In our research, we propose an approach to address the issue of inaccurate head BIFs by seeking a method based on simple data statistics to correct the BIF within the Patlak model. This article reports an initial study focused on this approach. Due to the limited availability of total-body dynamic PET data, we used only 67 datasets (with 64 used for data fitting, 3 for model testing, and cross-validation for validation). Notably, the amount of data include in this study is insufficient to guarantee fully stable and accurate pharmacokinetic parameter imaging using the Patlak graphical model. From a theoretical standpoint, we can reasonably assume that our proposed method is less dependent on the dataset size than machine learning-based methods. However, the size of the fitting dataset still unavoidably affects the algorithm's performance. Therefore, further expansion of the dataset is necessary to conduct a more comprehensive evaluation of the proposed method and enhance its stability and reliability in clinical applications.

Influence of patient head motion

Movement of the patient's head during the dynamic PET scan can affect the accuracy of brain parametric imaging, and in severe cases, it can lead to calculation failure. The method proposed in our study does not address this issue. In general, we pick up and sketch the cavernous sinus in one single frame (frame A) in the dynamic series, the acquire position and shape of the cavernous sinus would not be applicable in another frame (frame B) if head motion exist between the scanning timestamps of A and B, which lead to that the BIF signal acquired in frame B is not exactly from the cavernous sinus.

Therefore, for both the data fitting and testing processes, we needed datasets with no noticeable head motion and image framewise misalignment. This is an important reason why the amount of data available for the current study is limited. However, in conditions of clinical short-axis PET dynamic imaging, if parametric imaging is used for brain diagnosis, clinical technicians will require the patients to minimize voluntary head movement during the scanning process. In this case, the impact of head motion on the accuracy of parametric imaging can be controlled to some extent.

Tracer types

The current proposes a new method to correct the BIF extracted from the cavernous sinus. To validate the method using different types of tracers such as PSMA and FAPI-based tracers is necessary before this method is

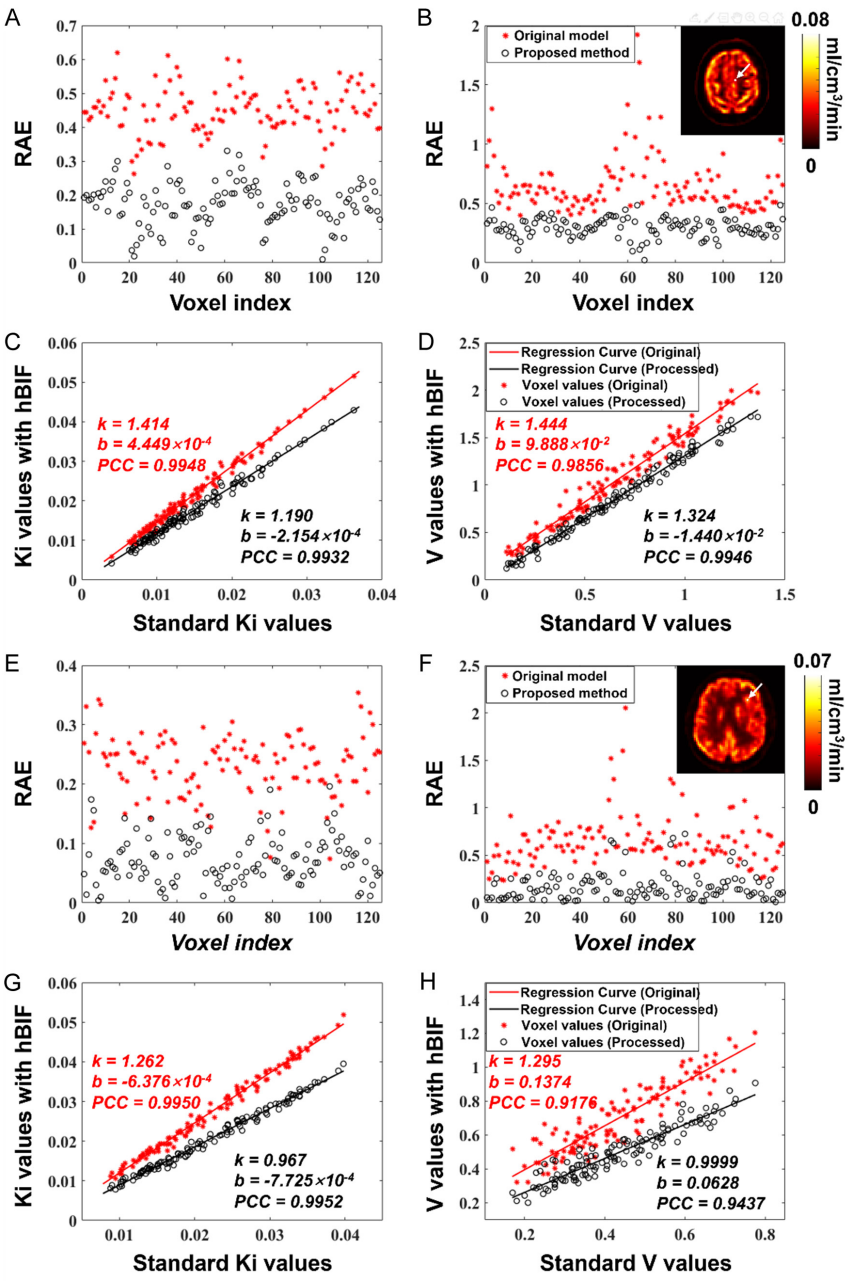

Figure 8. Accuracy evaluations performed with VOI-based analysis. (A and B) are the voxel RAEs within the 5 × 5 × 5 VOI in the K_i and V images, respectively, for tested dataset #5; (C and D) are the fitting results between the hBIF-based and aBIF-based parameter values within the same VOI; (E-H) correspond to tested dataset #14. The locations of the analyzed VOIs are indicated by the arrows in (B) and (F) for datasets #5 and #15, respectively.

promoted. However, since the protocol of dynamic PET scan is not routinely used in clinic, it is not easy to obtain dynamic PET data of the head using other tracers in the current study. Since the proposed method is established via statistical inductions based on a certain amount of image data, for a single tracer, insufficient amount of data will lead to failures of the algorithm. Therefore, As far as data we can access, the construction and evaluation of the framework are carried out based on only ^{18}F-FDG dynamic PET patient data.

Clinical relevance of the proposed method

The proposed method for correcting hBIF acquire based on cavernous sinus is able to facilitate clinical brain pharmacodynamic imaging and analysis. For many clinical institutes, PET scanners with long axial FOV (AFOV) are not equipped, under such case, it's impossible to acquire a standard BIF for brain pharmacodynamic analysis based on dynamic PET imaging since the AFOV is locked at the head region. The proposed method is to help clinicians to acquire a standard BIF for FDG dynamic PET Patlak parametric imaging when only head dynamic PET data are collected.

Conclusion

In this study, we propose a method for accurate brain Patlak pharmacokinetic parametric imaging using a cavernous sinus BIF. This method is established based on estimating the early-stage integral value and late-stage curve of the standard descending aorta BIF from the cavernous sinus BIF within the Patlak graphical model. Parametric imaging is achieved based on a modified Patlak model equation. Compared with the direct use of the cavernous sinus BIF, the proposed method is able to effectively improve the accuracy of K_i and V images of the brain and solve the problem of insufficient BIF accuracy under short-axis PET scanning conditions. The proposed method has high theoretical interpretability, and by effectively expanding the size of the database, it can actually improve the clinical applications of pharmacokinetic parametric imaging technology in the diagnosis of brain diseases.

Acknowledgements

This work was supported by the Key-Area Research and Development Program of Guangdong Province (2023-B0303030002), Guizhou province high-level innovative talents "Thousands of levels" personnel training project (GZSYQCC(2023)004), National Natural Science Foundation of China (62101540, 12305409) and Guangdong Basic and Applied Basic Research Foundation (2022-A1515110696).

Written informed consent was obtained from each subject for publication of their data and images.

Disclosure of conflict of interest

None.

Address correspondence to: Zhanli Hu, Lauterbur Research Center for Biomedical Imaging, Shenzhen Institute of Advanced Technology, Chinese Academy of Science, Shenzhen 518055, Guangdong, China. E-mail: zl.hu@siat.ac.cn; Yang Yu, School of Pharmaceutical Sciences, Guangzhou University of Chinese Medicine, Guangzhou 510006, Guangdong, China. E-mail: yuyang@gzucm.edu.cn

References

[1] Peng S, Tang C, Schindlbeck K, Rydzinski Y, Dhawan V, Spetsieris PG, Ma Y and Eidelberg D. Dynamic 18F-FPCIT PET: quantification of Parkinson's disease metabolic networks and nigrostriatal dopaminergic dysfunction in a single imaging session. J Nucl Med 2021; 62: 1775-1782.

[2] Seshadri V, Zarroli KA, Schetlick RS, Massey JC, Reyes JM, Eluvathingal Muttikal TJ, Patrie JT, Berr SS, Fountain NB, Kundu BK and Quigg M. Dynamic FDG-PET in localization of focal epilepsy: a pilot study. Epilepsy Behav 2021; 122: 108204.

[3] Quigg M and Kundu B. Dynamic FDG-PET demonstration of functional brain abnormalities. Ann Clin Transl Neurol 2022; 9: 1487-1497.

[4] Okazawa H, Ikawa M, Jung M, Maruyama R, Tsujikawa T, Mori T, Rahman MGM, Makino A, Kiyono Y and Kosaka H. Multimodal analysis using [(11)C]PiB-PET/MRI for functional evaluation of patients with Alzheimer's disease. EJNMMI Res 2020; 10: 30.

[5] Stephens K. New imaging approach could help stop epileptic seizures. AXIS Imaging News 2021.

[6] Zaragori T, Ginet M, Marie PY, Roch V, Grignon R, Gauchotte G, Rech F, Blonski M, Lamiral Z, Taillandier L, Imbert L and Verger A. Use of static and dynamic [18F]-F-DOPA PET parameters for detecting patients with glioma recurrence or progression. EJNMMI Res 2020; 10: 56.

[7] Karakatsanis NA, Zhou Y, Lodge MA, Casey ME, Wahl RL, Zaidi H and Rahmim A. Generalized whole-body Patlak parametric imaging for enhanced quantification in clinical PET. Phys Med Biol 2015; 60: 8643-73.

[8] Patlak CS, Blasberg RG and Fenstermacher JD. Graphical evaluation of blood-to-brain transfer constants from multiple-time uptake data. J Cereb Blood Flow Metab 1983; 3: 1-7.

[9] Wang G, Rahmim A and Gunn RN. PET parametric imaging: past, present, and future. IEEE Trans Radiat Plasma Med Sci 2020; 4: 663-675.

[10] Chen Z, Cheng Z, Duan Y, Zhang Q, Zhang N, Gu F, Wang Y, Zhou Y, Wang H, Liang D, Zheng H and Hu Z. Accurate total-body Ki parametric imaging with shortened dynamic 18F-FDG PET scan durations via effective data processing. Med Phys 2023; 50: 2121-2134.

[11] Rahmim A, Lodge MA, Karakatsanis NA, Panin VY, Zhou Y, McMillan A, Cho S, Zaidi H, Casey ME and Wahl RL. Dynamic whole-body PET imaging: principles, potentials and applications. Eur J Nucl Med Mol Imaging 2019; 46: 501-518.

[12] Chen J, Chen T, Fang Q, Pan C, Akakuru OU, Ren W, Lin J, Sheng A, Ma X and Wu A. Gd2O3/b-TiO2 composite nanoprobes with ultra-high photoconversion efficiency for MR image-guided NIR-II photothermal therapy. Exploration (Beijing) 2022; 2: 20220014.

[13] Dimitrakopoulou-Strauss A, Pan L and Sachpekidis C. Kinetic modeling and parametric imaging with dynamic PET for oncological applications: general considerations, current clinical applications, and future perspectives. Eur J Nucl Med Mol Imaging 2021; 48: 21-39.

[14] Guo J, Zhao Z, Shang ZF, Tang Z, Zhu H and Zhang K. Nanodrugs with intrinsic radioprotective exertion: turning the double-edged sword into a single-edged knife. Exploration (Beijing) 2023; 3: 20220119.

[15] Alberts I, Hünermund JN, Prenosil G, Mingels C, Bohn KP, Viscione M, Sari H, Vollnberg B, Shi K, Afshar-Oromieh A and Rominger A. Clinical performance of long axial field of view PET/CT: a head-to-head intra-individual comparison of the Biograph Vision Quadra with the Biograph Vision PET/CT. Eur J Nucl Med Mol Imaging 2021; 48: 2395-2404.

[16] Badawi RD, Shi H, Hu P, Chen S, Xu T, Price PM, Ding Y, Spencer BA, Nardo L, Liu W, Bao J, Jones T, Li H and Cherry SR. First human imaging studies with the EXPLORER total-body PET scanner. J Nucl Med 2019; 60: 299-303.

[17] Pantel AR, Viswanath V, Daube-Witherspoon ME, Dubroff JG, Muehllehner G, Parma MJ, Pryma DA, Schubert EK, Mankoff DA and Karp JS. PennPET Explorer: human imaging on a whole-body imager. J Nucl Med 2020; 61: 144-151.

[18] Mahalingam HV, Mani SE, Patel B, Prabhu K, Alexander M, Fatterpekar GM and Chacko G. Imaging spectrum of cavernous sinus lesions with histopathologic correlation. Radiographics 2019; 39: 795-819.

[19] Wanderi K and Cui Z. Organic fluorescent nanoprobes with NIR-IIb characteristics for deep learning. Exploration (Beijing) 2022; 2: 20210097.

[20] Pantel AR, Viswanath V, Muzi M, Doot RK and Mankoff DA. Principles of tracer kinetic analysis in oncology, part I: principles and overview of methodology. J Nucl Med 2022; 63: 342-352.

[21] Ding Y, Wang Y and Hu Q. Recent advances in overcoming barriers to cell-based delivery systems for cancer immunotherapy. Exploration (Beijing) 2022; 2: 20210106.

[22] Dai H, Fan Q and Wang C. Recent applications of immunomodulatory biomaterials for disease immunotherapy. Exploration (Beijing) 2022; 2: 20210157.

[23] Hudson HM and Larkin RS. Accelerated image reconstruction using ordered subsets of projection data. IEEE Trans Med Imaging 1994; 13: 601-609.

[24] Hsu H and Lachenbruch PA. Paired t test. Wiley StatsRef: statistics reference online. 2014.

[25] Lyu N, Pedersen B, Shklovskaya E, Rizos H, Molloy MP and Wang Y. SERS characterization of colorectal cancer cell surface markers upon anti-EGFR treatment. Exploration (Beijing) 2022; 2: 20210176.

[26] Sedgwick P. Pearson's correlation coefficient. BMJ 2012; 345: e4483.